OPTICAL REVIEW Vol. 13, No. 4 (2006) 283–287

Experimental Research on Focusing Property of Radially Polarized Beam Based on Solid Immersion Lens

Qing LI, Jia WANG*, Jiying XU, Jiefeng XI and Guofan JIN

State Key Laboratory of Precision Measurement Technology and Instruments, Department of Precision Instruments, Tsinghua University, Beijing 100084, P. R. China

(Received November 15, 2005; Accepted April 7, 2006)

Realization of a near-field optical virtual probe based on an evanescent Bessel beam is strongly dependent on a radially polarized beam; this makes it essential to study the focusing property of the beam. In this paper, two experimental setups based on a fiber device and a liquid crystal device, respectively, are built to generate a radially polarized beam. This beam and an annular radially polarized beam are focused by means of a high numerical aperture objective and a solid immersion lens (SIL). Near-field distribution of the focus spot, the evanescent Bessel field, is experimentally measured with a scanning near-field optical microscope (SNOM). The full width at half maximum (FWHM) of the central peak of the evanescent Bessel field is about 200 nm in the close vicinity of the bottom surface of SIL. This has potential for use as a near-field optical virtual probe. © 2006 The Optical Society of Japan

Key words: near-field optics, solid immersion lens (SIL), radially polarized beam, evanescent Bessel beam, virtual probe

1. Introduction

Mansfields and Kino[1)] proposed a solid immersion lens (SIL) method for high-resolution imaging. It is also used in high-density storage based on near-field optics because of its compatibility and high throughput. However, it is difficult to control separation down to tens of nanometers between optical pickup and disk with SIL technology. A near-field optical virtual probe based on an evanescent Bessel beam is a novel solution for near-field optical technology with SIL.

Grosjean and Courjon[2)] proposed the concept of the virtual tip in 2001. Based on the destructive combination of transverse magnetic (TM) polarized evanescent light beams, confined intensity distributions can be generated and do not vary versus the distance. Hong *et al.*[3)] obtained a simulation result of a virtual probe based on the interference of evanescent waves by means of the finite difference time domain (FDTD) method in 2002. Because an evanescent Bessel beam has diffraction-free property[4,5)] and achievable super resolution of the evanescent field, it is an ideal virtual probe. It can be produced by a radially polarized beam. Via evanescent Bessel beam, in 2003 Grosjean *et al.*[6)] first demonstrated both theoretical and experimental results dealing with the virtual probe. They found a very interesting property of Bessel beams and dependence of the ultimate resolutions on the polarization. Jia *et al.*[7)] investigated a tightly focused evanescent field produced by a total internal reflection objective lens under the illumination of a radially polarized beam generated using a single liquid crystal (LC) phase modulator; the field distributions were directly mapped by a scanning near-field optical microscope (SNOM).

In this paper, based on SIL, an evanescent Bessel beam has been obtained by focusing an annular radially polarized beam. Characteristics of the focusing properties of a radially polarized beam and an annular radially polarized beam were experimentally investigated, and some quantitative results on optical resolution beyond the diffraction limit are presented.

*E-mail address: wj-dpi@mail.tsinghua.edu.cn

2. Generation of Radially Polarized Beam

Several methods to generate a radially polarized beam have been proposed. Both an all-fiber device[8,9)] and a discontinuous phase element (DPE)[10,11)] can be used to generate such a beam. By introducing a spiral phase retardation plate in the interferometer,[12)] a radially polarized beam also can be produced by a suitable combination of constructive interference. In addition, a linearly polarized beam can be directly converted into a radially polarized beam by an LC device.[13)] A radially polarized beam can also be obtained by a polarization converter that consists of four half-wave plates.[14)] Even though it is not perfect in this polarization mode, tip-enhanced Raman spectroscopy is detected and some results were obtained by Hayazawa *et al.*[15)] Two methods based on a modified bi-mode fiber device and an elaborate LC device are described here to generate a high quality radially polarized beam.

2.1 Based on fiber device

A schematic diagram of an experimental setup for generating a radially polarized beam based on a fiber device is shown in Fig. 1. A beam from a He–Ne laser with 15 mW output power is first expanded and then converted into a circularly polarized beam by means of a quarter wave plate. Then it is coupled into a bi-mode fiber of a specific length with a 20× objective (N.A. = 0.4). The center of the focus spot is deviated in a certain displacement from the core of the bi-mode fiber in the direction perpendicular to the incident direction. The TE_{01} mode and TM_{01} mode are selected and emitted from the other end of the fiber. The beam is converted into a radially polarized beam by passing two half wave plates. The fiber characterized by a cutoff

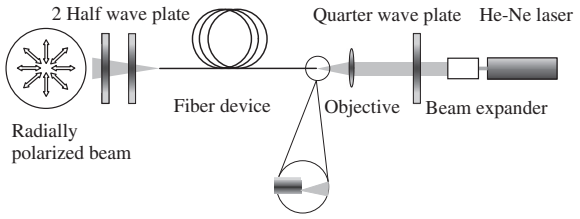

Fig. 1. Schematic diagram of the experimental setup for generating a radially polarized beam based on a fiber device.

wavelength (for the fundamental mode) of 730 ± 70 nm is designed for a single-mode fiber with wavelength of 820 nm and N.A. = 0.12. Here, for an incident light with a wavelength of 632.8 nm, the fiber can be used as a bi-mode fiber by calculating the normalized frequency.

In the experiment, the incident power of the focus spot into the bi-mode fiber is $P_{\text{input}} = 10.7$ mW. When the incident beam is a left-hand circularly polarized light, the output power of the bi-mode fiber is $P_{\text{output}} = 130\,\mu$W, and converting efficiency is $\eta = 1.21\%$. When the incident beam is a right-hand circularly polarized light, the output power is $P_{\text{output}} = 75\,\mu$W, and converting efficiency is $\eta = 0.701\%$. After passing the two half wave plates, the beam exiting from the bi-mode fiber is converted into the radially polarized beam, which is detected with a charge-coupled device (CCD) as shown in Fig. 2.

The experimental result indicates that the radially polarized beam generated by the fiber device is an annular beam and its intensity in the central region is weaker, even present a dark region in Fig. 2(a). The low coupling efficiency of the fiber results in low beam converting efficiency, so intensity of the radially polarized beam is weak. The positioning and adjusting errors in the fiber mode selection in the experimental setup cause an imperfect symmetry and the dark region of the obtained beam. Adjustments in the experiment are time-consuming and tedious.

2.2 *Based on LC device*

Under exterior action, an LC molecule will be moved so that its optical properties are varied; an LC device can therefore be constructed. As shown in Fig. 3, an LC device based on a twisted nematic effect and a specially designed LC cell for generation of an axially symmetrical polarized beam was proposed by Yamaguchi *et al.*[13] in 1989.

A schematic diagram of the experimental setup for

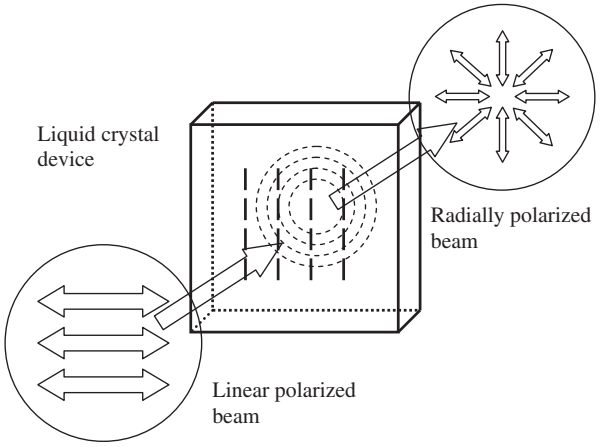

Fig. 3. Working principle of an LC device specially designed for generation of a radially polarized beam.

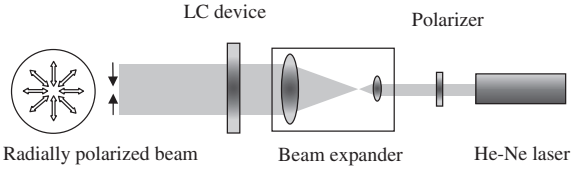

Fig. 4. Schematic diagram of the experimental setup for generating a radially polarized beam based on an LC device.

generating a radially polarized beam based on an LC device is shown in Fig. 4. The beam from a He–Ne laser with 30 mW output power first passes a polarizer in the horizontal direction, and then passes a 5× expander to enlarge the linearly polarized beam to 8 mm in diameter. The beam is normally incident upon the LC device, and the input beam is converted into a radially polarized beam after passing the LC device.

An elaborate LC device with a thickness of 20 μm and an area of $25 \times 25\,\text{mm}^2$ is used in the experiment. The input power of the LC device is $P_{\text{input}} = 10$ mW, the output power is $P_{\text{output}} = 3.29$ mW, and the converting efficiency is $\eta = 32.9\%$. The obtained radially polarized beam is detected by CCD as shown in Fig. 5.

Distribution of the radially polarized beam generated by the LC device is full, i.e., the central region is not dark and the spot is an intact circular spot. Experimental results indicate that the central part of the beam is not perfectly

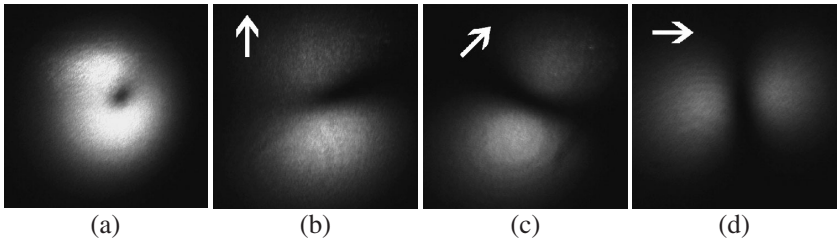

Fig. 2. Radially polarized beam generated by fiber device. (a) Radially polarized beam. (b), (c), (d) Intensity profiles of a radially polarized beam after passing through an analyzer. The arrows indicate the analyzer transmission axis.

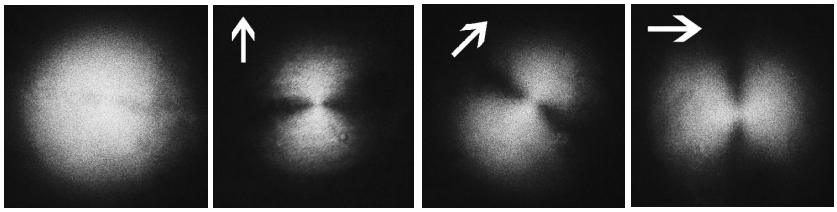

Fig. 5. Radially polarized beam generated by LC device. (a) Radially polarized beam. (b), (c), (d) Intensity profiles of a radially polarized beam after passing through an analyzer. The arrows indicate the analyzer transmission axis.

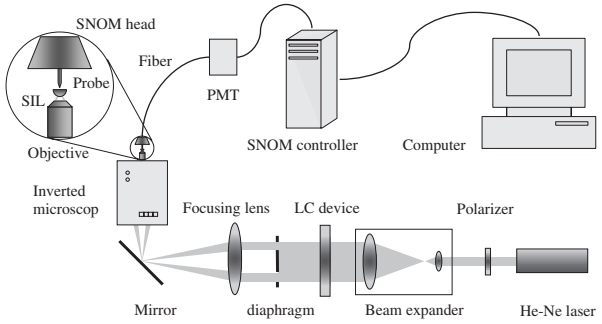

Fig. 6. Schematic diagram of an experimental setup for generating an evanescent Bessel beam based on SIL.

radially polarized and should be filtered in practical use. Overall, the radially polarized beam generated by the LC device has better symmetry and higher converting efficiency than that generated by the fiber device. In the subsequent experiment, therefore, the LC device is used to generate a radially polarized beam.

3. Generation and Measurement of Evanescent Bessel Beam Based on SIL

3.1 Experimental setup

A schematic diagram of the experimental setup for generating an evanescent Bessel beam by an SIL and a high N.A. objective with an incident radially polarized beam based on the LC device is shown in Fig. 6. A diaphragm with an aperture transmission function as eq. (1) follows the LC device to obtain an annular radially polarized beam.

$$G(\rho) = \begin{cases} 1 & \rho \text{ (mm)}; \ 3.0 \le \rho \le 4.0 \\ 0 & \rho \text{ (mm)}; \ \rho < 3.0, \ \rho > 4.0 \end{cases} \quad (1)$$

In eq. (1), ρ is radius of the diaphragm, and $G(\rho)$ is transmission efficiency of the diaphragm. The SIL is made of *K9* glass with refractive index 1.516 and the radius is 1.504 mm.

Under this condition, only a beam beyond the critical angle, an inhomogeneous field, can be focused on the bottom surface of the SIL. No homogeneous beam passes the SIL. The annular radially polarized beam is focused on the bottom surface of the SIL by a long working distance 100× objective with N.A. = 0.8. Two evanescent fields in opposite directions are generated and interfere with each other on the bottom surface of the SIL, resulting in the generation of evanescent Bessel field distribution.

An SNOM (from NT-MDT, Russia) is employed to observe the focus spot, the evanescent Bessel field distribution, in the vicinity of the bottom surface of the SIL. A tapered aluminum-coated fiber probe with a diameter of 100 nm is used to scan the field and collect the optical intensity signal.

3.2 Experimental result and discussion

For comparison, three kinds of polarized beams: a linearly polarized beam, a radially polarized beam without a diaphragm, and an annular radially polarized beam with a diaphragm are used in the experiments. The intensity distributions of all focus spots on the SIL bottom surface are mapped by a SNOM using the same optical fiber probe, as shown in Figs. 7–9.

For the incident linearly polarized beam, full width at half maximum (FWHM) of the measured focus spot on the SIL bottom surface is about 540×520 nm, approaching the diffraction limit, as shown in Fig. 7. The distribution of the focus spot does not show obvious elongation along the polarization direction as symmetrical incidence. Although SIL is used, the optical focusing system still is limited by the diffraction. Any improvement on resolution cannot be beyond the Rayleigh criterion. The homogeneous field still dominates in the focusing beam. Improvement of imaging resolution is dependent on the parameters of SIL, refractive index and geometry.

For the incident radially polarized beam, FWHM of the measured focus spot on the SIL bottom surface is about 430×390 nm, 75–80% of the focus spot with the linearly polarized beam under the same conditions, as shown in Fig. 8. Although there is diffusion around the spot, its size still is close to the diffraction limit. The homogeneous field caused by the beam inside the critical angle and the inhomogeneous field caused by the beam beyond the critical angle are generated at the same time. The homogeneous field still dominates in the focusing beam. However, the focus spot is obviously smaller than the linearly polarized beam. Several blur red spots are around the focus spot. The reason may be due to scattering of the flaw of optical components and adjusting error.

For the incident annular radially polarized beam, the FWHM of the measured focus spot on the SIL bottom surface is about 230×180 nm, as shown in Fig. 9. It is considerably less than the diffraction limit, 35–45% of the focus spot of the linearly polarized beam under the same conditions. In this case, all of the incident beams beyond the critical angle are focused onto the SIL/air interface and satisfy the total internal reflection condition. Only the

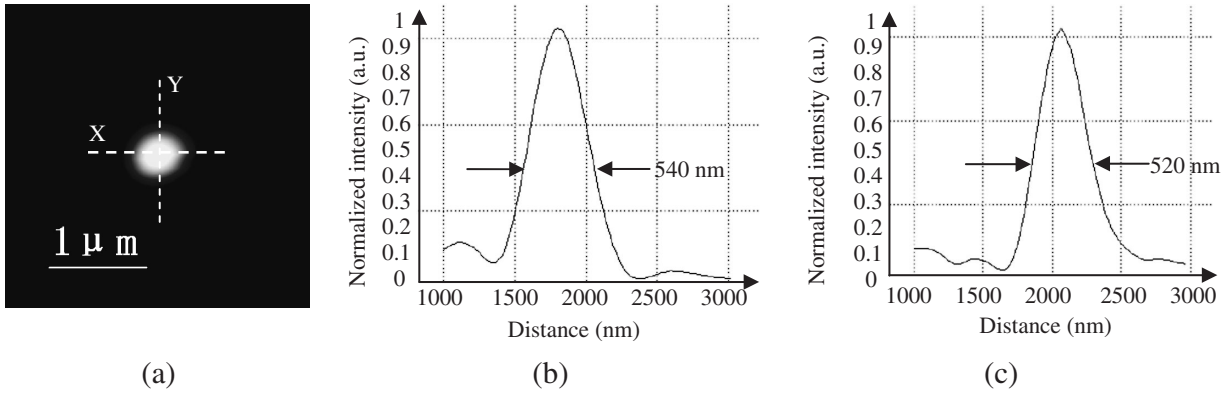

Fig. 7. Measured focus spot by SIL with incident linearly polarized beam. (a) Intensity distribution on the SIL bottom surface. (b) Intensity along the *X* direction. The FWHM is 540 nm. (c) Intensity along the *Y* direction. The FWHM is 520 nm.

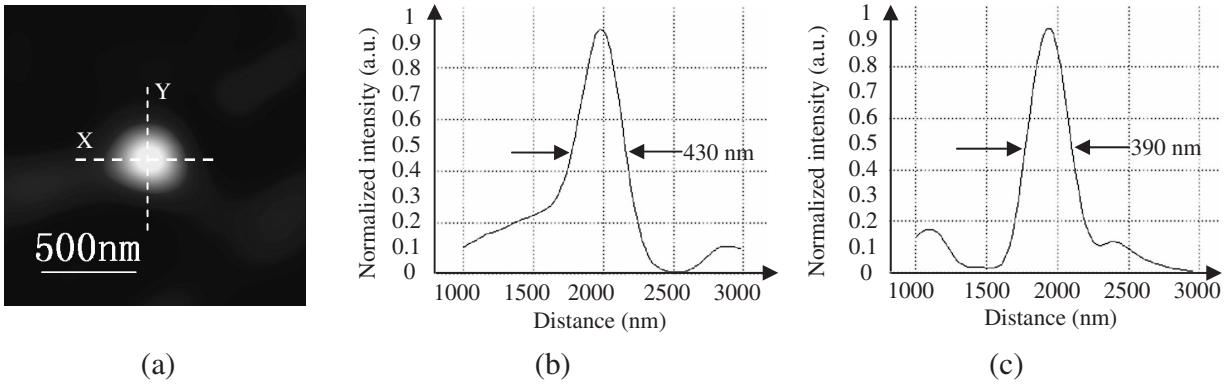

Fig. 8. Measured focus spot by SIL with incident radially polarized beam. (a) Intensity distribution on the SIL bottom surface. (b) Intensity along the *X* direction. The FWHM is 430 nm. (c) Intensity along the *Y* direction. The FWHM is 390 nm.

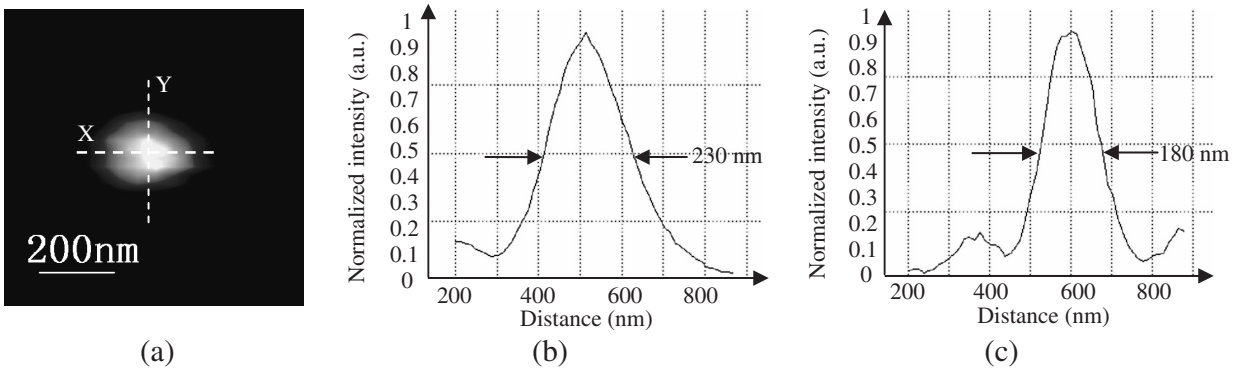

Fig. 9. Measured focus spot by SIL with incident annular radially polarized beam, i.e., evanescent Bessel beam. (a) Intensity distribution on the SIL bottom surface. (b) Intensity along the *X* direction. The FWHM is 230 nm. (c) Intensity along the *Y* direction. The FWHM is 180 nm.

inhomogeneous field can be focused. The evanescent Bessel field distribution is generated on the bottom surface of the SIL, which can be used as a near-field virtual probe. The spot distribution is anomalous, and shows obvious elongation along the *X* direction, which may be due to the imperfections of optical components and adjusting errors.

4. Conclusion

A radially polarized beam with cylindrical symmetry is obtained experimentally. Employment of a radially polarized beam in the experiments indicates that it has better focusing property than a common linearly polarized beam and obtains a smaller spot beyond the diffraction limit in the experimental setup based on an SIL. Based on the principle of evanescent field interference, an evanescent Bessel beam is experimentally obtained on the SIL bottom surface with an annular radially polarized beam. FWHM of its main spot size is about 200 nm, considerably less than the focus spot with the common linearly polarized beam. This is a feasible method to realize a near-field virtual probe. Instead of the conventional optical probe, it can increase power-transmitted efficiency and relax the critical condition for separation control in near-field optical imaging and storage systems.

Acknowledgments

The authors of the article appreciate support from the Chinese National Natural Science Foundation Project (No. 60278029).

They also gratefully acknowledge Professor Rumiko Yamaguchi from Akita University, Japan and Professor Yanqing Lian from Tsinghua University for discussions and fabrication of LC devices.

References

1) S. M. Mansfields and G. S. Kino: Appl. Phys. Lett. **57** (1990) 2615.
2) T. Grosjean and D. Courjon: J. Microsc. **202** (2001) 273.
3) T. Hong, J. Wang, L. Q. Sun and D. C. Li: Appl. Phys. Lett. **81** (2002) 3452.
4) J. Durnin: J. Opt. Soc. Am. A **4** (1987) 651.
5) J. Durnin, J. J. Miceli and J. H. Eberly: Phys. Rev. Lett. **58** (1987) 1499.
6) T. Grosjean, D. Courjon and D. Van Labeke: J. Microsc. **210** (2003) 319.
7) B. H. Jia, X. S. Gan and M. Gu: Opt. Express **13** (2005) 6821.
8) T. Grosjean, D. Courjon and M. Spajer: Opt. Commun. **203** (2002) 1.
9) G. Volpe and D. Petrov: Opt. Commun. **237** (2004) 89.
10) R. Oron, Y. Danziger, N. Davidson and A. A. Friesem: Appl. Phys. Lett. **74** (1999) 1373.
11) R. Oron, S. Blit, N. Davidson and A. A. Friesem: Appl. Phys. Lett. **77** (2000) 3322.
12) C. T. Steve, H. F. Dennis and D. K. Wayne: Appl. Opt. **29** (1990) 2234.
13) R. Yamaguchi, T. Nose and S. Sato: Jpn. J. Appl. Phys. **28** (1989) 1730.
14) R. Dorn, S. Quabis and G. Leuchs: Phys. Rev. Lett. **91** (2003) 233901.
15) N. Hayazawa, Y. Saito and S. Kawata: Appl. Phys. Lett. **85** (2004) 6239.